JACS
JOURNAL OF THE AMERICAN CHEMICAL SOCIETY
Communication
pubs.acs.org/JACS

Self-Assembled 2D Free-Standing Janus Nanosheets with Single-Layer Thickness

Yiyang Lin, Michael R. Thomas, Amy Gelmi, Vincent Leonardo, E. Thomas Pashuck, Stephanie A. Maynard, Ye Wang, and Molly M. Stevens*

Department of Materials, Department of Bioengineering and Institute of Biomedical Engineering, Imperial College London, Exhibition Road, London SW7 2AZ, U.K.

Supporting Information

ABSTRACT: We report the thermodynamically controlled growth of solution-processable and free-standing nanosheets via peptide assembly in two dimensions. By taking advantage of self-sorting between peptide β-strands and hydrocarbon chains, we have demonstrated the formation of Janus 2D structures with single-layer thickness, which enable a predetermined surface heterofunctionalization. A controlled 2D-to-1D morphological transition was achieved by subtly adjusting the intermolecular forces. These nanosheets provide an ideal substrate for the engineering of guest components (e.g., proteins and nanoparticles), where enhanced enzyme activity was observed. We anticipate that sequence-specific programmed peptides will offer promise as design elements for 2D assemblies with face-selective functionalization.

Two-dimensional (2D) nanostructures are an important material class with diverse potential applications.[1−4] It remains a challenge to produce free-standing 2D materials without a templating surface or confined space. Recently, covalent (e.g., click chemistry)[5−7] and noncovalent[8−12] strategies have been developed to construct 2D structures. Of particular interest are the biological units (e.g., protein, DNA, peptide, and peptoid) that can be engineered in a well-defined manner to favor self-assembly in 2D.[13−20] For example, homoligomeric 2D protein assemblies with spatial arrangements and patterns have previously been achieved by exploiting the directionality of metal coordination interactions.[13] However, although amphiphilic peptides represent an important class of supramolecular units with a proclivity toward aggregating into 1D nanomaterials (e.g., nanotubes and fibrils),[21−28] the design of 2D peptide structures is infrequently reported. This is because the H-bonding arising from amide groups dominates 1D peptide self-assembly preferentially along the direction parallel to H-bonding.

Herein, we construct 2D materials via the manipulation of peptide self-assembly in two dimensions (Figures 1a and S1). A peptide amphiphile **F6C11** containing hexa-phenylalanine, a hydrophobic tail, and glutamic acids was designed. The hexa-phenylalanine segment was incorporated to provide H-bonding to form β-sheets in the x-axial direction, with concomitant β-sheet stacking in the y-axial direction via aromatic interactions (Figure 1b).[24−26,29,30] The resulting self-assembly in 2D is consistent with previous studies where tyrosine and phenylalanine-rich peptides have been reported to form 2D nanobelts and nanosheets.[20,29] An alkyl tail was incorporated to strengthen the hydrophobic effect in both directions (x and y), where enthalpy (H)-governed self-sorting between hexa-phenylalanine and the alkyl tail enables us to create asymmetric peptide layers with the capability of heterofunctionalization on the opposing faces (Figure 1b).[31]

The aggregation of **F6C11** was confirmed by Nile Red fluorescence, where an increase of emission intensity and a spectral blue shift was observed, indicating the solubilization of Nile Red in a hydrophobic domain (Figure 1c). The solution of **F6C11** was found to be cloudy with low viscosity, suggesting the formation of large but multidimensional aggregates that scattered incident light strongly. Structured illumination microscopy (SIM), transmission electron microscopy (TEM), and tapping mode atomic force microscopy (AFM) revealed homogeneous nanosheets hundreds of nanometers wide and several microns long (Figures 1d−1f, S2). The observation of a fraction of overlapping plates suggested that they were free-standing in solution and stacked during sample preparation. In two overlapped sheets, the shape of the second layer can still be identified, indicating that the nanosheets were ultrathin. Indeed, AFM showed a homogeneous thickness of ∼5 nm, in agreement with the theoretical monolayer thickness. Overlapped nanosheets were also visualized by AFM, giving a surface height of ∼10 nm. The single-layer nanosheets could be easily isolated from solution by centrifugation and recovered by redispersion without affecting the nanosheet morphology and structural integrity (Figure S3). The recovery yield of nanosheets after a centrifugation/redispersion process was determined to be as high as 92%. Such a property is important for nanosheet separation, purification, and functionalization.

Synchrotron radiation small-angle X-ray scattering (SAXS) confirmed the plate-like configuration with a Q^{-2} decay in the Guinier region (Figure 1g, Table S1). A quantitative assessment of the thickness of the structures was accomplished by fitting the data as lamellar sheets and indicated a thickness of 4.8 nm. The mechanism of 2D self-assembly was characterized by circular dichroism (CD), Thioflavin T (ThT) assay, and Fourier transform infrared spectroscopy (FTIR). Strong CD signals were observed for F6C11 nanosheets (Figure 1h), where a minimum at 225 nm and a maximum at 202 nm are

Received: June 25, 2017
Published: September 13, 2017

DOI: 10.1021/jacs.7b06591
J. Am. Chem. Soc. 2017, 139, 13592−13595

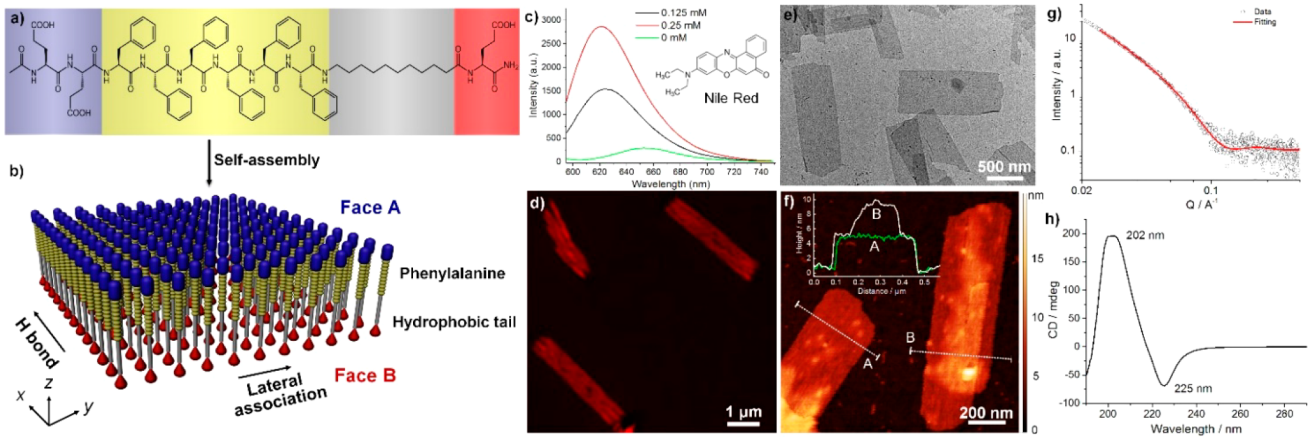

Figure 1. (a, b) Schematic of **F6C11** self-assembly into Janus nanosheets following self-sorting between phenylalanine (blue) and hydrocarbon tails (red). (c) Fluorescence spectra of Nile Red in the presence or absence of **F6C11**. (d) SIM, (e) TEM, (f) AFM images of nanosheets. The inset in (f) shows the height profile across the marked section indicated by A and B in (f). (g) SAXS profile plot for solution structures of nanosheets (black circles) and fit to lamellar sheets of thickness 4.8 nm (red trace). (h) CD spectrum of nanosheets.

representative of β-sheets. The minimum at 225 nm was red-shifted compared to ~216 nm of a typical β-sheet, due to the aromatic interactions between phenylalanine.[29,32,33] The FTIR spectrum of **F6C11** nanosheets exhibited the vibration peaks of amide I (1625 cm^{-1}) and amide II (1543 cm^{-1}), suggesting the parallel β-sheets (Figure S4). The ThT assay confirmed the existence of rigid β-sheets with an increase of fluorescence emission in nanosheets (Figure S5).

The surface of the nanosheets can selectively display specific reactive groups via coassembly of **F6C11** and functionalized peptides that share the same backbone (Figure S1). Since the main driving forces for 2D self-assembly originate from the configuration of the hexa-phenylalanine and hydrocarbon chains, the incorporation of nonionic groups is not supposed to alter the hydrophobicity/hydrophilicity balance or the self-assembly pathway. Indeed, the insertion of a biotinylated peptide (**Bio-F6C11**) did not cause notable morphological changes to the nanosheets (Figure 2a, b). The biotin-displaying nanosheets can be quantitatively decorated with streptavidin, a 52.8 kDa protein, via biotin−streptavidin affinity due to the high affinity (Figure S6). AFM imaging demonstrated small features that included a height ~5 nm, close to the size of a protein (Figure 2c, d); the thickness of nanosheets remained unchanged (~5 nm, Figure 2e).

The biotin-displaying nanosheets can be used as a substrate to immobilize enymes, e.g., avidin D-horseradish peroxidase (AvD-HRP) (Figure 2f) while retaining the enzyme activity. In the presence of H_2O_2, HRP catalyzed the oxidation of 3,3′,5,5′-tetramethylbenzidine (TMB) to produce a reaction product with an absorption at 650 nm. Interestingly, the immobilization of HRP on the nanosheets was found to increase the rate of catalytic reaction, which is not due to the intrinsic enzymatic activity of peptides (Figure 2g). A similar phenomenon was found when using negatively charged ABTS as a substrate (Figure S7). The enhanced enzymatic activity likely results from the highly negatively charged nanosheets acting to lower the local pH, which has previously been shown to increase the activity of HRP.[34]

Beyond biotin−avidin interactions, the peptide nanosheets can serve as a substrate to host inorganic nanomaterials (e.g., Au nanoparticles, quantum dots, Au nanorods) and fluorophores via thiol−Au bonding, electrostatic force, and copper-free click chemistry (Figures S8, S9).

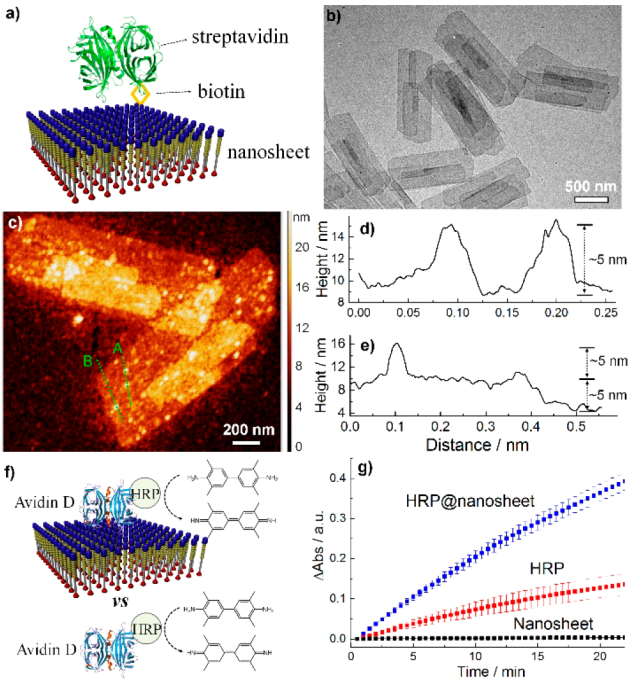

Figure 2. (a) Adsorption of streptavidin on a nanosheet. (b) TEM image of biotin-displaying nanosheets. (c) AFM image of streptavidin-anchored nanosheets. (d, e) AFM height profiles across nanosheet indicated as A and B in (c), respectively, suggesting the size of protein to be ~5 nm and the single-layer thickness of nanosheet. (f) Surface assembly of HRP on the nanosheet via biotin−avidin affinity, and HRP-catalyzed TMB oxidization. (g) Kinetics of HRP-catalyzed TMB oxidation by H_2O_2.

Due to the self-sorting between hexa-phenylalanine and the alkyl chain, the single-layered nanosheets possess two different surfaces, with N-termini on Face A and C-termini on Face B (Figure 1b). To confirm the Janus nature of the nanosheets and their surface heterofunctionalization, we incoporated biotin and cysteine on opposing faces, via co-assembly of **F6C11**, **Bio-F6C11**, and **F6C11-Cys**, and immobilized the nanosheets on a silicon wafer via the thiol−maleimide reaction. The biotin-

DOI: 10.1021/jacs.7b06591
J. Am. Chem. Soc. 2017, 139, 13592−13595

displaying face was therefore exposed to bulk solution and could be modified with streptavidin-coated AuNPs (Figure 3a, b). In contrast, the nanosheets displaying biotin and cysteine on the same surface (Surface A) could not be used to assemble streptavidin-AuNPs once they were anchored to the silicon wafer (Figure 3c, d) since the biotin moieties were embedded toward silicon and not exposed to solution. All together, we believe the peptide nanosheets are highly ordered with C-termini on one face and N-termini on the other, enabling the presentation of two different groups on opposing surfaces.

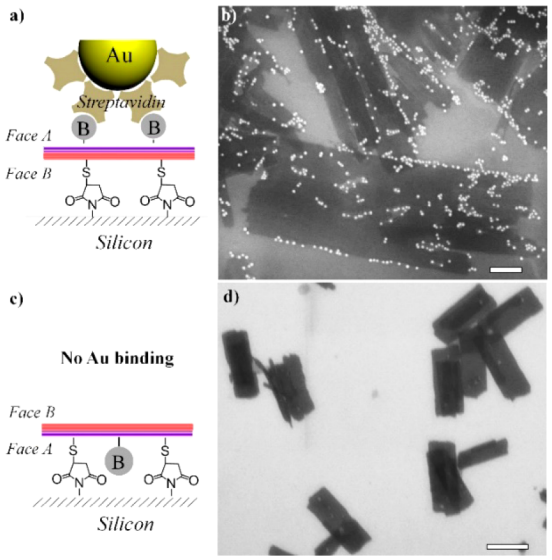

Figure 3. (a) Schematic and (b) scanning electron microscopy image showing nanosheets functionalized with cysteine and biotin (denoted as "B") on opposing faces can be immobilized on silicon surfaces and modified with streptavidin-AuNPs. (c) Schematic and (d) SEM image showing nanosheets with cysteine and biotin on the same surface did not undergo specific AuNP binding. Scale bar: (b) 200 nm; (d) 1 μm.

Peptide nanostructures of varied morphology could be formed by varying the peptide sequences. For example, twisted fibrils were formed by **F5C11** and **F4C11** (Figure 4a, b), when the number of phenylalanines was reduced to 5 and 4, respectively. This is because a reduction in the number of phenylalanines weakens the β-sheet stacking in the y-axial direction, resulting in the formation of 1D structures along the x-axial direction. Meanwhile, the electrostatic repulsions between terminal charges in **F4C11** and **F5C11** became overwhelming, which can favor the intrinsic twist of β-sheet.[29,35] Similarly β-sheet fibrils were formed when valine was substituted for phenylalanine (**V6C11**) (Figures 4c, S10). More subtly, the size of nanosheets in both dimensions could be reduced by shortening the alkyl chain from C_{11} to C_6, resulting in 2D plates with a width of ~178 nm and a length of ~1.05 μm (Figures 4d, S11). This can be rationalized since a shortening of the alkyl chain would reduce the hydrophobic interactions and therefore weaken the peptide association in both the x and y directions.

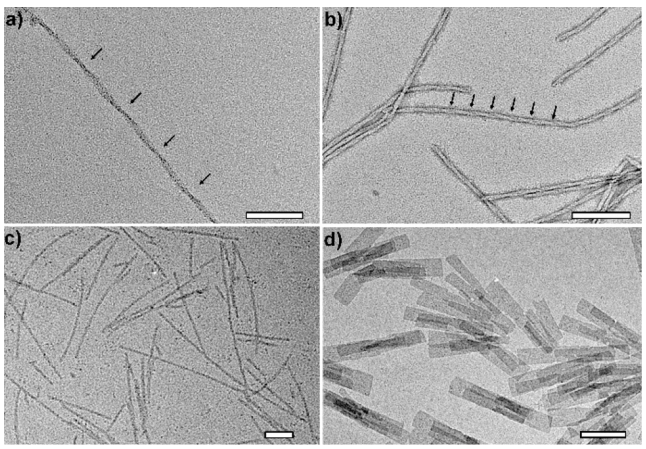

Figure 4. TEM images of nanostructures: (a) **F4C11**, (b) **F5C11**, (c) **V6C11**, and (d) **F6C6**. Scale bar: (a–c) 100 nm, (d) 500 nm. The arrows in (a) and (b) denote helical features of **F4C11** and **F5C11** fibrils, respectively.

These morphological transitions were accompanied by changes in internal ordering (e.g., β-sheet strength, micropolarity, and fluidity) of the peptide structures. As shown by ThT and Nile Red assays (Figure S12), the β-sheets were weakened and the micropolarity of the peptide structures was increased as the number of phenylalanines was reduced or substituted by valine (**F6C11** > **V6C11** > **F5C11** > **F4C11**). Similarly, shortening of the alkyl chain from C11 to C6 was also found to weaken β-sheet strength and increase micropolarity. The fluidity of the peptide layers was probed by fluorescence polarization (FP) using 1,6-diphenyl-1,3,5-hexatriene (DPH). The FP value of DPH was found to increase (**F6C11** ≈ **F6C6** ≈ **V6C11** > **F5C11** > **F4C11**) when more amide H-bonds were present, indicating the decisive role of amide bonds in determining the fluidity (Figure S13). We therefore propose that **F6C11** nanosheets display a high structural ordering cooperatively stabilized by H-bonding, aromatic stacking, and the hydrophobic effect as defined by the alkyl tail length, which compete with the electrostatic repulsion between glutamic acids.

In conclusion, we have designed Janus nanosheets with single-layer thickness via peptide self-assembly, which offers the possibility of dual functionalization on opposing surfaces. Benefiting from the versatility of surfaces displaying different reactive groups, the nanosheets can serve as substrates for various guest components. In particular, the surface-confined enzyme assembly on nanosheets was observed to enhance the catalytic activity, which can mimic the enzymatic reaction in living systems that take place at biological membranes. The important role of amino acid side groups (especially aromatic groups) was highlighted in promoting β-sheet stacking to favor peptide self-assembly in 2D. We anticipate these 2D Janus nanomaterials can be engineered with surface ligands (e.g., cell-targeting and analyte-binding properties) to inspire broad applications such as drug delivery and bioelectronic sensing.

■ ASSOCIATED CONTENT

Supporting Information

The Supporting Information is available free of charge on the ACS Publications website at DOI: 10.1021/jacs.7b06591.

Experimental details, ThT assay, SIM, Nile Red assay, FTIR, CD, and fluorescence polarization (PDF)

■ AUTHOR INFORMATION

Corresponding Author

*m.stevens@imperial.ac.uk

DOI: 10.1021/jacs.7b06591
J. Am. Chem. Soc. 2017, 139, 13592–13595

ORCID

Yiyang Lin: 0000-0003-2017-190X
Michael R. Thomas: 0000-0001-7795-9648
E. Thomas Pashuck: 0000-0003-2881-4965
Molly M. Stevens: 0000-0002-7335-266X

Notes

The authors declare no competing financial interest.
Raw data is available online at DOI: 10.5281/zenodo.888563.

■ ACKNOWLEDGMENTS

Imaging was performed in the Facility for Imaging by Light Microscopy (FILM), partly supported by the BBRSC [BB/L015129/1]. We acknowledge Diamond Light Source for provision of synchrotron beamtime, and we would like to thank Dr. Andy Smith and Dr. Hanna Barriga for assistance using beamline I22. A.G. was supported by the European Union's Horizon 2020 Research and Innovation Programme through the Marie Skłodowska-Curie Individual Fellowship "RAISED" [660757]. E.T.P. was supported by Marie Curie actions FP7 through the Intra-European Marie Curie Fellowship "Peptide Osteogel" [275433]. S.A.M. was supported by a Ph.D. studentship within Biomedicine and Bioengineering in Osteoarthritis. Y.W. was supported by the China Scholarship Council. M.M.S. acknowledges the Engineering and Physical Sciences Research Council (EPSRC) for the grant "Bio-functionalized Nanomaterials for Ultra-sensitive Biosensing" [EP/K020641/1]. M.M.S. and M.R.T. acknowledge support from the i-sense EPSRC IRC in Early Warning Sensing Systems for Infectious Diseases [EP/K031953/1]. M.M.S. and Y.L. acknowledge support from the ERC Seventh Framework Programme Consolidator Grant "Naturale CG" [616417].

■ REFERENCES

(1) Boott, C. E.; Nazemi, A.; Manners, I. *Angew. Chem., Int. Ed.* **2015**, *54*, 13876−13894.
(2) Colson, J. W.; Dichtel, W. R. *Nat. Chem.* **2013**, *5*, 453−465.
(3) Cai, S.-L.; Zhang, W.-G.; Zuckermann, R. N.; Li, Z.-T.; Zhao, X.; Liu, Y. *Adv. Mater.* **2015**, *27*, 5762−5770.
(4) Zhuang, X.; Mai, Y.; Wu, D.; Zhang, F.; Feng, X. *Adv. Mater.* **2015**, *27*, 403−427.
(5) Zheng, Y.; Zhou, H.; Liu, D.; Floudas, G.; Wagner, M.; Koynov, K.; Mezger, M.; Butt, H.-J.; Ikeda, T. *Angew. Chem., Int. Ed.* **2013**, *52*, 4845−4848.
(6) Bauer, T.; Zheng, Z.; Renn, A.; Enning, R.; Stemmer, A.; Sakamoto, J.; Schlüter, A. D. *Angew. Chem., Int. Ed.* **2011**, *50*, 7879−7884.
(7) Baek, K.; Yun, G.; Kim, Y.; Kim, D.; Hota, R.; Hwang, I.; Xu, D.; Ko, Y. H.; Gu, G. H.; Suh, J. H.; et al. *J. Am. Chem. Soc.* **2013**, *135*, 6523−6528.
(8) Hudson, Z. M.; Boott, C. E.; Robinson, M. E.; Rupar, P. A.; Winnik, M. A.; Manners, I. *Nat. Chem.* **2014**, *6*, 893−898.
(9) Kim, Y.; Shin, S.; Kim, T.; Lee, D.; Seok, C.; Lee, M. *Angew. Chem., Int. Ed.* **2013**, *52*, 6426−6429.
(10) Bai, W.; Jiang, Z.; Ribbe, A. E.; Thayumanavan, S. *Angew. Chem., Int. Ed.* **2016**, *55*, 10707−10711.
(11) Ni, B.; Huang, M.; Chen, Z.; Chen, Y.; Hsu, C.-H.; Li, Y.; Pochan, D.; Zhang, W.-B.; Cheng, S. Z. D.; Dong, X.-H. *J. Am. Chem. Soc.* **2015**, *137*, 1392−1395.
(12) Ishiba, K.; Noguchi, T.; Iguchi, H.; Morikawa, M.-a.; Kaneko, K.; Kimizuka, N. *Angew. Chem., Int. Ed.* **2017**, *56*, 2974−2978.
(13) Brodin, J. D.; Ambroggio, X. I.; Tang, C.; Parent, K. N.; Baker, T. S.; Tezcan, F. A. *Nat. Chem.* **2012**, *4*, 375−382.
(14) Yu, H.; Alexander, D. T. L.; Aschauer, U.; Häner, R. *Angew. Chem., Int. Ed.* **2017**, *56*, 5040−5044.
(15) Hughes, M.; Xu, H.; Frederix, P. W. J. M.; Smith, A. M.; Hunt, N. T.; Tuttle, T.; Kinloch, I. A.; Ulijn, R. V. *Soft Matter* **2011**, *7*, 10032−10038.
(16) Nam, K. T.; Shelby, S. A.; Choi, P. H.; Marciel, A. B.; Chen, R.; Tan, L.; Chu, T. K.; Mesch, R. A.; Lee, B.-C.; Connolly, M. D.; et al. *Nat. Mater.* **2010**, *9*, 454−460.
(17) Mannige, R. V.; Haxton, T. K.; Proulx, C.; Robertson, E. J.; Battigelli, A.; Butterfoss, G. L.; Zuckermann, R. N.; Whitelam, S. *Nature* **2015**, *526*, 415−420.
(18) Jiang, T.; Xu, C.; Liu, Y.; Liu, Z.; Wall, J. S.; Zuo, X.; Lian, T.; Salaita, K.; Ni, C.; Pochan, D.; et al. *J. Am. Chem. Soc.* **2014**, *136*, 4300−4308.
(19) Jang, H.-S.; Lee, J.-H.; Park, Y.-S.; Kim, Y.-O.; Park, J.; Yang, T.-Y.; Jin, K.; Lee, J.; Park, S.; You, J. M.; et al. *Nat. Commun.* **2014**, *5*, 3665.
(20) Min, K.-I.; Yun, G.; Jang, Y.; Kim, K.-R.; Ko, Y. H.; Jang, H.-S.; Lee, Y.-S.; Kim, K.; Kim, D.-P. *Angew. Chem., Int. Ed.* **2016**, *55*, 6925−6928.
(21) Wei, G.; Su, Z.; Reynolds, N. P.; Arosio, P.; Hamley, I. W.; Gazit, E.; Mezzenga, R. *Chem. Soc. Rev.* **2017**, *46*, 4661.
(22) Hartgerink, J. D.; Beniash, E.; Stupp, S. I. *Proc. Natl. Acad. Sci. U. S. A.* **2002**, *99*, 5133−5138.
(23) Lamm, M. S.; Rajagopal, K.; Schneider, J. P.; Pochan, D. J. *J. Am. Chem. Soc.* **2005**, *127*, 16692−16700.
(24) Reches, M.; Gazit, E. *Science* **2003**, *300*, 625−627.
(25) Adamcik, J.; Castelletto, V.; Bolisetty, S.; Hamley, I. W.; Mezzenga, R. *Angew. Chem., Int. Ed.* **2011**, *50*, 5495−5498.
(26) Yan, X.; Zhu, P.; Li, J. *Chem. Soc. Rev.* **2010**, *39*, 1877−1890.
(27) Li, S.; Mehta, A. K.; Sidorov, A. N.; Orlando, T. M.; Jiang, Z.; Anthony, N. R.; Lynn, D. G. *J. Am. Chem. Soc.* **2016**, *138*, 3579−3586.
(28) Gao, Y.; Zhao, F.; Wang, Q.; Zhang, Y.; Xu, B. *Chem. Soc. Rev.* **2010**, *39*, 3425−3433.
(29) Hu, Y.; Lin, R.; Zhang, P.; Fern, J.; Cheetham, A. G.; Patel, K.; Schulman, R.; Kan, C.; Cui, H. *ACS Nano* **2016**, *10*, 880−888.
(30) Castelletto, V.; Hamley, I. W.; Hule, R. A.; Pochan, D. *Angew. Chem., Int. Ed.* **2009**, *48*, 2317−2320.
(31) Yu, Z.; Tantakitti, F.; Palmer, L. C.; Stupp, S. I. *Nano Lett.* **2016**, *16*, 6967−6974.
(32) Gazit, E. *FASEB J.* **2002**, *16*, 77−83.
(33) Bowerman, C. J.; Liyanage, W.; Federation, A. J.; Nilsson, B. L. *Biomacromolecules* **2011**, *12*, 2735−2745.
(34) Zhang, Y.; Tsitkov, S.; Hess, H. *Nat. Commun.* **2016**, *7*, 13982.
(35) Adamcik, J.; Mezzenga, R. *Soft Matter* **2011**, *7*, 5437−5443.

DOI: 10.1021/jacs.7b06591
J. Am. Chem. Soc. 2017, 139, 13592−13595